Available online at www.sciencedirect.com
ScienceDirect
Journal of the European Ceramic Society 29 (2009) 2643–2650
www.elsevier.com/locate/jeurceramsoc

Capillary infiltration studies of liquids into 3D-stitched C–C preforms Part A: Internal pore characterization by solvent infiltration, mercury porosimetry, and permeability studies

Suresh Kumar [a,*], Anil Kumar [a], Anupam Shukla [b], A.K. Gupta [b], Rohini Devi [a]

[a] *Advanced Systems Laboratory (DRDO), Hyderabad 500058, India*
[b] *Department of Chemical Engineering, IIT Delhi, New Delhi 110016, India*

Available online 14 April 2009

Abstract

Mathematical modeling of silicon infiltration in porous carbon–carbon (C–C) preforms is the key to fabricate liquid silicon infiltration based carbon–silicon carbide (C–SiC) composite components. Existing models for silicon infiltration are based on straight capillaries. For interconnected capillary systems, e.g. as in 3D-stitched C–C preforms these show large deviations when compared with experimental observations. The aim of the present study is to develop a mathematical model suitable for silicon infiltration in 3D-stitched C–C preforms. The work is being presented in two parts: A and B. This part (Part A) describes the experimental details pertaining to the fabrication of the C–C preforms and their pore structure characterization by mercury porosimetry, infiltration of solvents by capillary rise, and by permeability studies. A two-pore capillary infiltration model termed as modified Washburn equation has been proposed. It has been validated by experimental data of solvent infiltration. The same model correlates silicon infiltration observations as well (Part B).

Keywords: Composites; Modeling

1. Introduction

Ceramic–matrix composites are promising materials for hypersonic aircrafts and for hot structures of re-entry vehicles.[1,2] Liquid-silicon-infiltration (LSI) based carbon–silicon carbide (C–SiC) composites have short manufacturing cycles.[3,4] However most of the work has been carried out on monolithic (reaction bonded) silicon carbide and 2D C–SiC composites. Experimental observations of silicon infiltration in carbon–carbon (C–C) preforms are limited, and the mathematical models for infiltration are based on straight capillaries.[5–8]

3D composites exhibit better thermal and mechanical properties under severe erosion and complex mechanical loading conditions, e.g. thrust vectoring jet-vanes, leading edges of hypersonic vehicles, etc.[2,3] 3D-stitched composites are easy to fabricate and can be used for such applications. Understanding of infiltration dynamics of molten silicon in C–C preforms is essential for the development of LSI based C–SiC composites. Direct observation of silicon infiltration in C–C components is not possible because of high temperature 1450–1650 °C and vacuum conditions. To make use of the existing capillary infiltration models, effective mean pore radius of C–C preform is required. An experimental method based on capillary rise is widely used for porous-medium characterization. Measurement of the penetration height of wetting liquid with time is most commonly employed.[7,9–12] Darcy's law has also been employed to characterize a porous medium by measuring downward liquid flow under static and dynamic liquid heads.[13]

It is desirable to study the pore structure of the 3D-stitched C–C preforms before modeling of silicon infiltration is attempted. To characterize such preforms, mercury porosimetry, capillary infiltration of solvents, and permeability studies have been proposed. Information thus obtained would give a deep insight into their pore structure. Thus, the objectives of this part of the study are: (1) to fabricate 3D-stitched-C–C preforms of density range 1.55–1.60 g/cm^3, and (2) to understand their pore structure. To achieve (2), the following were decided:

1. to determine pore-size distribution;
2. to carry out solvent infiltration studies with four different organic solvents;

* Corresponding author. Tel.: +91 40 24306498; fax: +91 40 24306498.
E-mail address: sureshtanwar@rediffmail.com (S. Kumar).

0955-2219/$ – see front matter © 2009 Elsevier Ltd. All rights reserved.
doi:10.1016/j.jeurceramsoc.2009.03.007

3. to determine permeability;
4. to arrive at an appropriate mathematical model for solvent infiltration and to analyze the experimental data.

2. Experimental

2.1. Raw materials

T300 carbon-fiber reinforcement in the form of 8H satin 3k woven fabric and 6k tows were used to make 3-D-stitched fibrous performs. Low quinoline-soluble coal-tar pitch was used for densification of the fibrous preforms. Laboratory grade solvents were used; these were procured from Merck (India).

2.2. C–C preform development

Many 3D-stitched fibrous preforms (150 mm × 150 mm, and 50 mm thick) were prepared by stitching several layers of carbon fabric with carbon-fiber tows. These preforms were infiltrated with coal-tar pitch by vacuum infiltration (absolute pressure = 1×10^{-3} mmHg, i.e. 0.13 Pa) at 200–300 °C followed by carbonization at 900–1000 °C and graphitization at 2500–2600 °C in nitrogen atmosphere. These were further densified by hot-iso-static-pitch impregnation and carbonization at 750–800 °C and 100 MPa. The densified preforms were further heat-treated at 1650 °C under vacuum (absolute pressure = 1×10^{-3} mmHg). The C–C preforms thus obtained had a density range 1.55–1.60 g/cm^3. The heating rate was controlled to maintain the temperature increase at 50–100 °C/h in all the above steps.

2.3. Internal pore structure characterization

2.3.1. Pore-size distribution using mercury porosimetry

Specimens of size 25 mm × 5 mm × 5 mm were cut from the above C–C preforms for determination of pore-size distribution and porosity. Measurements were carried out as per ASTM D-2873 up-to 30,000 psi (~200 MPa) using Quantachrome Instruments. Volume of mercury intruded as a function of the applied pressure was recorded (Figs. 1 and 2). A typical pore-size distribution is shown in Fig. 3.

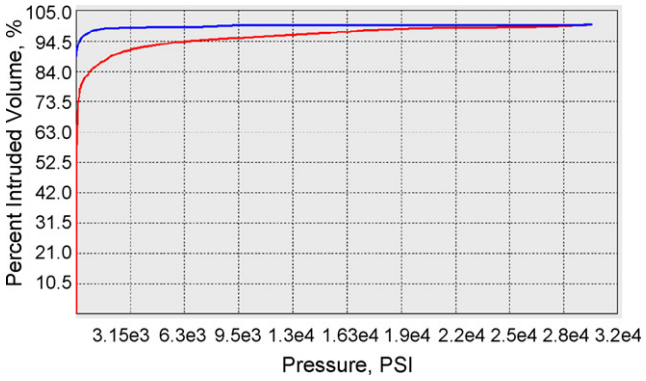

Fig. 1. Percentage mercury volume intruded vs. applied pressure.

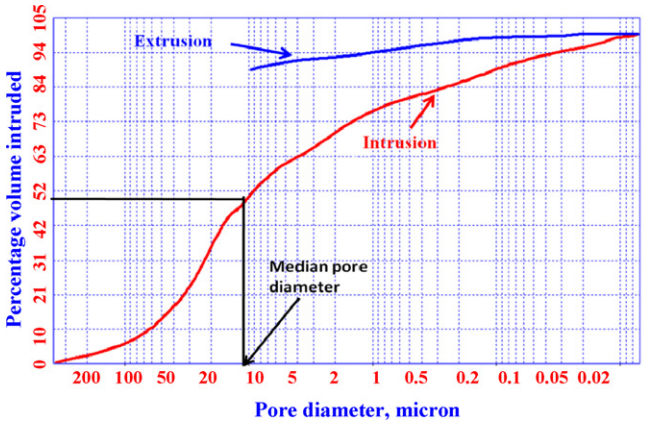

Fig. 2. Percentage mercury volume intruded vs. pore diameter.

Observations for one specimen are given below:

Volume of specimen	0.5472 cm^3
Volume of mercury intruded	0.1162 cm^3
Pore diameter range	0.007–400 μm
Porosity	21.23%
Median pore diameter (on the basis of volume)	8.6 μm

2.3.2. Capillary infiltration of solvents

Four blocks of size 150 mm × 50 mm × 50 mm were cut from different C–C preforms. These were used for preliminary infiltration studies with acetone. Outer surface of the blocks was graduated at the intervals of 5 mm in the direction parallel to the fabric. The graduated blocks were just dipped up to a depth of 1–2 mm in acetone contained in a Petri-dish. It was observed that acetone rose upwards quickly. Acetone was added to the Petri-dish to maintain its level. The height of acetone front was noted with time. A schematic of the capillary rise is shown in Fig. 4.

Experiments were also attempted with water for capillary infiltration, but without any success.

Detailed studies were carried out with four different solvents, viz. acetone, ethyl alcohol, cyclohexanone, and cyclohexane, with the same C–C preform block. The infiltration behavior of all the four solvents was similar (Fig. 5). Observations for ethyl alcohol are given in Table 1. Initially solvents rose very fast; however infiltration front was not uniform; perhaps, due to the local pore structure. As time progressed infiltration front became

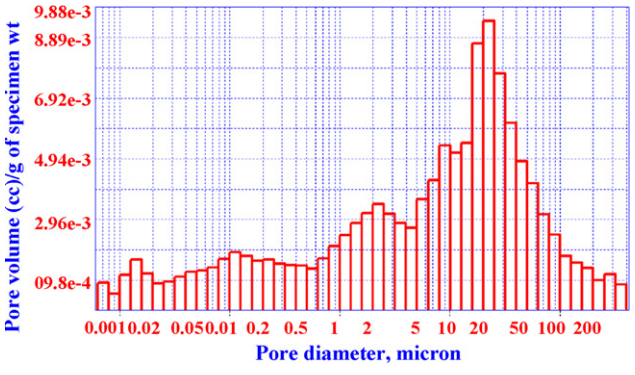

Fig. 3. Pore-size distribution of a C–C preform sample.

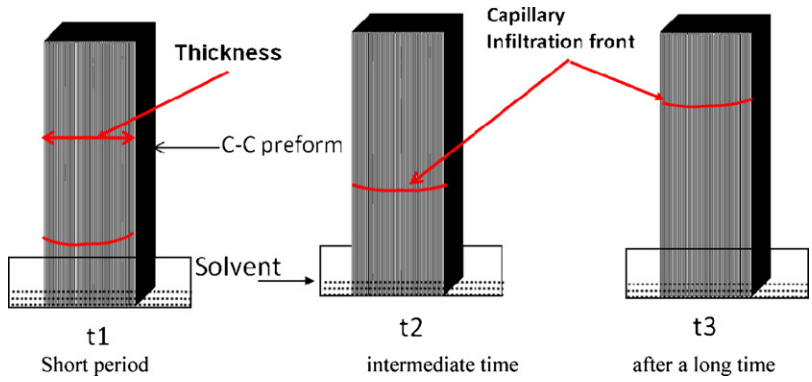

Fig. 4. Schematic of capillary rise into C–C preform block.

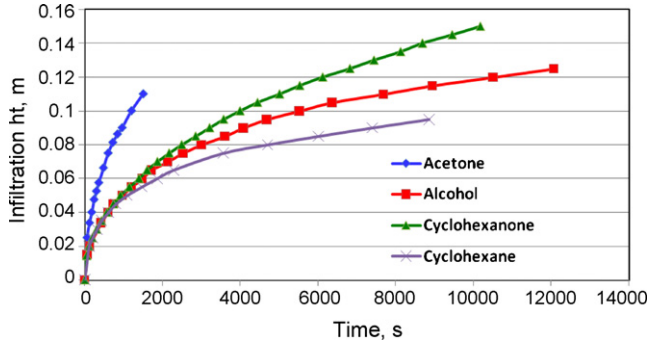

Fig. 5. Capillary infiltration heights for solvents.

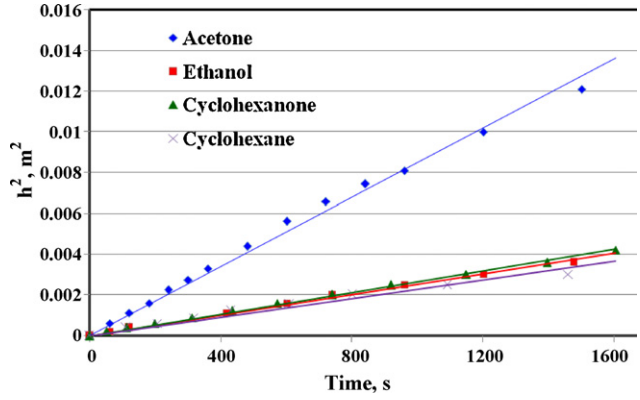

Fig. 6. Variation of square of capillary infiltrated heights of solvents with time for C–C preform block.

uniform, and also the rate of infiltration became slow. Measurements were discontinued after a sufficiently long time when further rise was not observed. For acetone infiltration height could not be measured beyond 115 mm; it was very difficult to differentiate the infiltration front from the shade of C–C preform block. Perhaps it was due to high rate of evaporation and very slow infiltration rate.

Solvents rise in the C–C preform by capillary action. The rate of rise depends upon the pore radius, properties of the solvents viz. density, viscosity, surface tension, and its angle of contact with the pore walls. Densities of these solvents are not much different. Since all the studies were carried out with the same C–C preform block, viscosity, surface tension, and angle of contact would control the rate of rise. It may be noted that viscosity of acetone is the least among the four solvents; its rate of rise is also the highest.

It has been reported in literature[9,12,14] that during the initial periods

$$h^2 \propto t \quad (1)$$

where h is the infiltration height in the capillary, t is the infiltration time and h^2 was plotted for all the solvents against time (Fig. 6).

It can be observed that during initial periods, h^2 varies linearly with time.

2.3.3. Permeability measurements

To characterize the C–C preforms further permeability was measured in the direction parallel to fabric layers. The observations would give cumulative effect of all pores under downward flow.

2.3.3.1. Experimental set-up (Fig. 7). It consisted of a flanged hollow tube of square cross section, 44 mm × 44 mm. Height of the tube above the flange was 1 m and below the flange, it was 15 mm. A C–C preform of thickness 5–10 mm could be mounted inside the lower tube.

Table 1
Ethyl alcohol capillary heights in C–C preform block.

Time, s	0	60	120	420	600	738	960	1200	1476
Infiltration height, m	0	0.015	0.02	0.034	0.04	0.045	0.05	0.055	0.06
Time, s	1716	2136	2526	3000	3600	4080	4680	5520	6360
Infiltration height, m	0.065	0.07	0.075	0.08	0.085	0.09	0.095	0.10	0.105
Time, s	7680	8940	10500	12060	–	–	–	–	–
Infiltration height, m	0.11	0.115	0.120	0.125	–	–	–	–	–

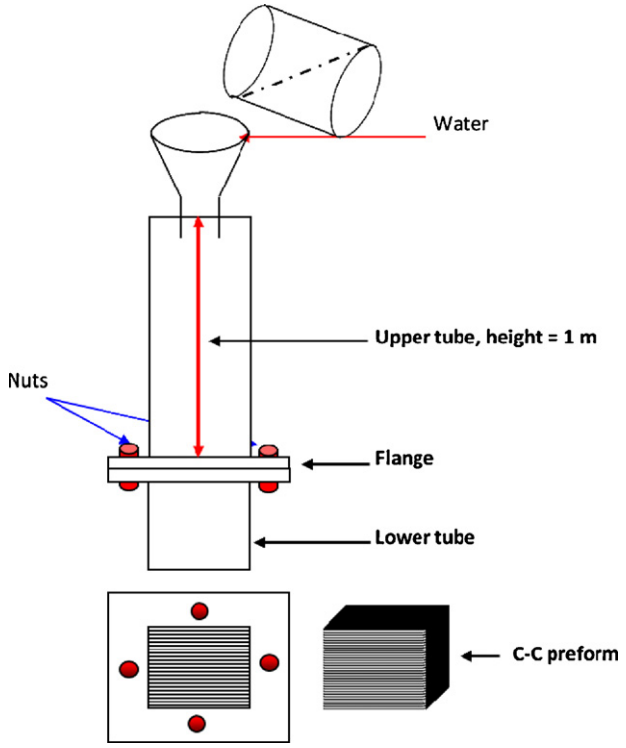

Fig. 7. Experimental set-up for permeability measurement of C–C preform sample.

2.3.3.2. Procedure. A C–C preform specimen of thickness 7.1 mm was flush-mounted in the lower tube. The edges of the specimen were sealed to the inner walls of the tubes with epoxy resin to prevent any leakage from the sides. Both the tubes were assembled by tightening nuts and bolts. The assembly was mounted on an angle-frame. Water was filled in the tube from the top. The water head above the C–C preform specimen was maintained 1 m throughout the experiment. The water coming out from the lower end was measured at intervals of two minutes. This was continued till constant volumetric flow rate was achieved (Table 2).

2.3.3.3. Determination of permeability. Steady state volumetric flow rate data were used to determine the value of permeability.

$$\vartheta = \frac{\kappa}{\mu}\frac{dP}{dx} = \frac{\kappa}{\mu}\frac{\Delta P}{l} \tag{2}$$

where ϑ is the average superficial velocity of water, 'κ' is the permeability, ΔP is the pressure drop across the thickness of the preform specimen l, and μ is the viscosity of water.

Volumetric flow of water at steady state = 655×10^{-6} m^3/s. Taking $\mu = 1.0 \times 10^{-3}$ kg/m s, the value of the permeability (κ) was calculated to be 2.04×10^{-12} m^2.

Studies were carried out for specimens of different thicknesses as well; the permeability values were found to be in the range 1.98×10^{-12} to 2.2×10^{-12} m^2. In the present calculations permeability has been taken to be 2.04×10^{-12} m^2. Subsequently this value of κ was used to estimate solvent infiltration height.

2.3.3.4. Effective mean pore diameter under down ward flow. A C–C preform may be considered equivalent to a bundle of straight, unconnected, parallel capillaries of uniform pore radius. Hagen Poiseuille equation relates pressure drop for laminar flow in a cylindrical capillary of length (l) and mean effective capillary diameter (d)

$$\frac{\Delta P}{l} = \frac{32u\mu}{d^2} \tag{3}$$

where μ is the average velocity of liquid in the capillary.

If ε is the porosity of the specimen, (ϑ) may be defined as

$$\vartheta = u \times \varepsilon \tag{4}$$

Porosity (ε) was determined by immersing the C–C preform specimen in water for a long time. Weight of the preform was taken before and after immersing it into water.

$$\text{Porosity} = \frac{\text{volume of the water penetrated}}{\text{volume of the preform}}$$

It was found to be 0.15.

It may be noted that the porosity as measured by mercury porosimetry was 0.2133. It indicates that fine pores were not filled completely by water. From Eqs. (2)–(4), the diameter (d) may be expressed as

$$d = \sqrt{\left(\frac{32\kappa}{\varepsilon}\right)} \tag{5}$$

Substituting for $\kappa = 2.04 \times 10^{-12}$ m^2 and $\varepsilon = 0.15$, d was found to be 20.8×10^{-6} m. Thus, effective mean pore radius (r_d) under downward flow is 10.4×10^{-6} m.

2.4. Analysis of solvent infiltration observations

As mentioned earlier, there are two approaches to analyze capillary infiltration data, viz. Darcy's law and Washburn equation.[8,12–14]

Table 2
Observations of a permeability experiment.

Time interval, min	0–2	2–4	4–6	6–8	8–10	10–12	12–14	14–16	16–18
Volume of water collected, ml	1000	950	895	850	810	780	765	751	739
Time interval, min	18–20	20–22	22–24	24–26	26–28	28–30	30–32	32–34	34–36
Volume of water collected, ml	739	729	720	709	694	680	660	655	655

2.4.1. Darcy's law applied to upward capillary infiltration

Darcy's law for one-dimensional capillary infiltration may be written as

$$\vartheta = \frac{\kappa}{\mu}(\nabla P - \rho g) \tag{6}$$

where ∇P is the pressure gradient due to capillary pressure, g is acceleration due to gravity and ρ is the density of the liquid.

Eq. (6) may be re-written as

$$\vartheta = \frac{\kappa}{\mu}\left(\frac{\Delta P}{h} - \rho g\right) \tag{7}$$

or

$$\vartheta = \frac{\kappa}{\mu h}(\Delta P - \rho g h) \tag{8}$$

or

$$h\vartheta = \frac{\kappa}{\mu}(\Delta P - \rho g h) \tag{9}$$

where h = infiltration height at any time t.

Substituting for upward velocity, $\vartheta = dh/dt$ in Eq. (9), we get

$$h\frac{dh}{dt} = \frac{\kappa}{\mu}(\Delta P - \rho g h) \tag{10}$$

The capillary pressure ΔP can be determined independently. Eq. (10) was solved to estimate capillary height for all the four solvents (Figs. 11–14). There is a good agreement between the estimated and experimental values.

2.4.2. Washburn equation

Momentum balance for liquid rising through a single capillary can be written as

Rate of change of momentum

$$= \sum \text{the driving forces} = \text{capillary force}$$

$$-\text{gravitational force} - \text{viscous force}.$$

or

$$\frac{d}{dt}\left(\pi r^2 h\rho\frac{dh}{dt}\right) = \left(\frac{2\sigma\cos\theta}{r} - \rho g h - \frac{8\mu h}{r^2}\frac{dh}{dt}\right)\pi r^2 \tag{11}$$

where dh/dt is the upward velocity of the liquid in the capillary.

Simplifications:

(i) For capillaries of small radii creeping flow assumption may be applied; it implies that $(d/dt)(h(dh/dt))$ is very small and approaches zero.

Thus the above equation may be re-written as

$$\frac{8\mu h}{r^2}\frac{dh}{dt} = \frac{2\sigma\cos\theta}{r} - \rho g h \tag{12}$$

(ii) Also during initial periods, $\rho g h \ll (8\mu h/r^2)(dh/dt)$.

Eq. (12) can be re-written as

$$\frac{8\mu h}{r^2}\frac{dh}{dt} = \frac{2\sigma\cos\theta}{r} \tag{13}$$

The above equation implies that, during initial period capillary pressure is balanced by viscous drag.

Integrating Eq. (13) and simplifying

$$h^2 = \frac{r\sigma\cos\theta}{2\mu}t \tag{13a}$$

2.4.2.1. Determination of effective mean pore radius for C–C preform. Substituting for slopes of the plots of h^2 vs. t (Fig. 6) and physical properties of solvents[15] into Eq. (13a), effective mean radius was determined (Table 3). It was found to be 0.274 μm.

It may be noted that effective mean pore radius as 0.274 μm is much smaller than 10.4 μm determined from permeability experiments and than 4.3 μm determined from mercury porosimetry. It should also be noted that there is a wide pore-size distribution in the C–C preform.

2.4.2.2. Estimation of capillary height. Infiltration heights for all the four solvents were estimated for capillaries of different radii arrived at by different approaches (i) 0.274 μm (Eq. (13a)), (ii) 10.4 μm (from permeability observations), and (iii) 4.3 μm from mercury porosimetry. The estimated heights for all the solvents showed large deviations from the experimental observations (Fig. 8).

It is evident that larger the pore radius, higher would be the rate of rise during the initial period, infiltration would stop after attaining a height h_∞ where gravity force balances capillary pressure.

Table 3
Physical properties of solvents and slopes of h^2 vs. t plot.

Solvents	Density (kg/m^3)	Viscosity (kg/m s)	Surface tension (N/m)	Slope	$r\cos(\theta)$	θ (°)	Effective radius (μm)
Acetone	770	0.30×10^{-3}	23.70×10^{-3}	9.0×10^{-6}	2.28×10^{-7}	33	0.274
Ethyl alcohol	780	1.07×10^{-3}	22.60×10^{-3}	2.2×10^{-6}	2.08×10^{-7}	40	0.274
Cyclohexane	780	0.92×10^{-3}	24.65×10^{-3}	2.0×10^{-6}	1.49×10^{-7}	57	0.274
Cyclohexanone	948	1.99×10^{-3}	34.00×10^{-3}	2.2×10^{-6}	2.57×10^{-7}	20	0.274

Note: Since solvent infiltration studies were carried out with the same C–C preform block; there would be a unique value for radius for all the solvents. Angle of contact for different solvents was adjusted to obtain the same value for radius in all the cases.

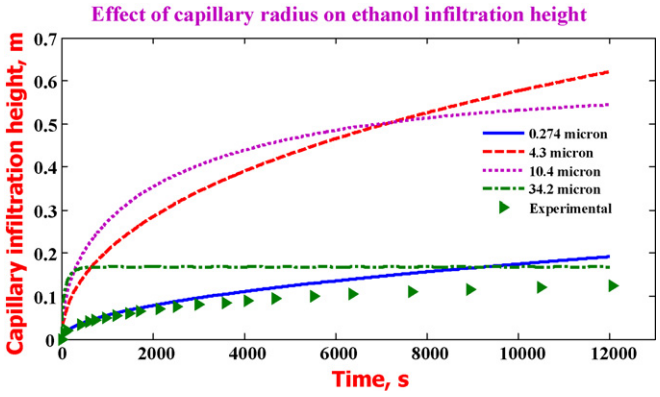

Fig. 8. Effect of pore radii on infiltration height for ethyl alcohol calculated using Eq. (13a).

Table 4
Theoretical capillary infiltration heights of ethyl alcohol for different pore radii.

Radius 'r', μm	0.274	10.4	4.3	34.2
h_∞, m	17.0	0.447	1.08	0.135

Maximum capillary height h_∞ which may be attained by a solvent by capillary rise can be determined.[16,17]

$$h_\infty = \frac{2\sigma\cos\theta}{\rho g r} \tag{14}$$

h_∞ for ethyl alcohol for different pore radii are listed in Table 4.

It is evident that heights (17.0, 0.447, and 1.08 m) estimated for radii 0.274, 10.4 and 4.3 μm respectively are much higher than the experimental value (0.135 m). The effective pore radius responsible for capillary pressure would be about 34 μm. Also, infiltration height is a function of time cannot be determined using Eq. (12) based on a single value of capillary radius. This observation necessitated looking at the mechanism of capillary infiltration being controlled by pores of more than one size. This is discussed in the next section.

3. Physical picture envisaged for 3D-stitched C–C preforms

3D stitched C–C preform is a layered porous structure; typical thickness of carbon fabric and carbon matrix in the preform is about 0.25 mm each. The preforms have a wide range of pore sizes (Fig. 3). The schematic of the thickness of a C–C preform and the interconnected capillaries is shown in Fig. 9. There are two types of pores: (i) those in the carbon matrix between different fabric layers and (ii) in the carbon matrix entrapped in the fabric itself. These have been termed as (i) coarse pores 'm' (for matrix) and fine pores 'f' (for fabric). The pores 'm' are coarse because of non-uniform shrinkage characteristic of the carbon matrix. In the 3D stitched C–C preforms, the third direction carbon-fibers hold different fabric layers and do not allow the entire preform to shrink uniformly during carbonization; thus larger pores 'm' get generated in the matrix whereas 'f' pores are created in the matrix trapped in the fabrics. The coarse and the fine pores are inter-connected. As the liquid rises up through

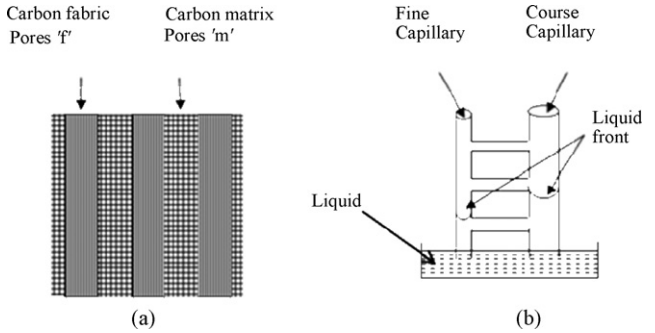

Fig. 9. (a) Schematic of side view of C–C preform, and (b) interconnected capillary infiltration scheme.

the C–C preform block, a complex interflow of infiltrating liquid takes in the pores.

3.1. Capillary infiltration into interconnected complex pore structure

It is very likely that effective pore size responsible for viscous drag is different from the effective pore size responsible for capillary pressure. Assuming this hypothesis and considering pores of two different radii (a) one responsible for capillary pressure and (b) the other for viscous drag following phenomenon is proposed.

During initial stages of infiltration, height of liquid in the coarse pores would be higher than that in the fine pores because of difference in viscous drag. The pores are interconnected; hence some of the liquid from the coarse pores would flow into fine pores to maintain equal level in the preform. Later, static head and capillary pressure in the coarse pores would tend to become equal resulting in no further rise of the liquid in the coarse pores. For fine pores, however, capillary pressure is higher than the static head, therefore liquid rise through these would continue and then it flows to coarse pores. But, height of the liquid in the coarse pores cannot exceed beyond the value where the capillary force and static head are in equilibrium. Therefore maximum infiltration height (h_∞) by capillary action in such cases would be controlled mainly by the coarse pores.

During the initial periods, the viscous drag in the fine pores is much higher than that in the coarse pores; therefore, fine pores control the infiltration velocity. Hence for analysis of capillary infiltration, both types of pores (coarse and fine) should be taken into consideration.

3.2. Modified Washburn equation

Denoting effective radius of coarse pores as r_1, effective radius of pores for viscous drag as r_2 and substituting $r = r_1$ for capillary pressure and $r = r_2$ for viscous flow, Eq. (12) can be re-written as

$$0 = \left(\frac{2\sigma\cos\theta}{r_1} - \rho g h - \frac{8\mu h}{r_2^2}\frac{dh}{dt}\right)$$

or

$$\left(\rho g h + \frac{8\mu h}{r_2^2}\frac{dh}{dt}\right) = \frac{2\sigma\cos\theta}{r_1} \tag{15}$$

This is termed as modified Washburn equation.

Eq. (15) can be used to determine solvent infiltration height as a function of time if the values of radii r_1 and r_2 are known.

(i) As $t \to \infty$, $h \to h_\infty$ and $dh/dt \to 0$
Therefore Eq. (15) reduces to

$$\rho g h_\infty = \frac{2\sigma\cos\theta}{r_1} \tag{16}$$

Solving Eq. (16) for r_1

$$r_1 = \frac{2\sigma\cos\theta}{\rho g h_\infty} \tag{17}$$

r_1 can be determined by measuring maximum capillary height (h_∞) and substituting for physical properties of the solvent.

Note: h_∞ measured for cyclohexane was 0.1 m. r_1 was determined from Eq. (17), it was found to be 34.2 μm. Since solvent infiltration studies were carried out with the same C–C preform block, there would be a unique value of r_1 for other solvents also.

h_∞ was calculated for other solvents as well. The value for acetone, ethyl alcohol, and cyclohexanone was 0.159, 0.136, and 0.2 m respectively.

(ii) r_2 must represent pores of all sizes for combined viscous drag; hence it may be assumed to be equal to the median pore radius obtained from mercury porosimetry. Its value was 4.3 μm.

(iii) Thus at any time 't', the Eq. (15) may be re-written as

$$\frac{8\mu}{r_2^2}\frac{h\,dh}{dt} - \frac{2\sigma\cos\theta}{r_1} + \rho g h = 0 \tag{15a}$$

(iv) Special case, $t \to 0$, $h \to 0$

Eq. (15) reduces to

$$\frac{8\mu h}{r_2^2}\frac{dh}{dt} = \frac{2\sigma\cos\theta}{r_1}$$

which on integration and simplifying, becomes

$$h^2 = \frac{r_2^2}{r_1}\frac{\sigma\cos\theta}{2\mu}t \tag{13b}$$

or, $$\frac{h^2}{t} = \frac{r_2^2}{r_1}\frac{\sigma\cos\theta}{2\mu}$$

For acetone, ethyl alcohol, cyclohexane, and cyclohexanone the value of the R.H.S. is 17.88×10^{-6}, 4.37×10^{-6}, 3.94×10^{-6}, and 4.33×10^{-6} respectively. The values of the slope reported in Table 3 are $9.0 \times 10^{-6}, 2.2 \times 10^{-6}, 2.0 \times 10^{-6}$, and 2.2×10^{-6} respectively, which are almost one half of the values of h^2/t at $t \to 0$.

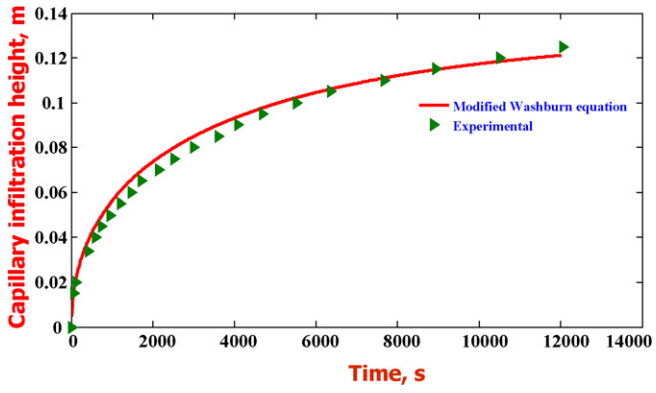

Fig. 10. Comparison of estimated and experimental infiltration heights of ethyl alcohol.

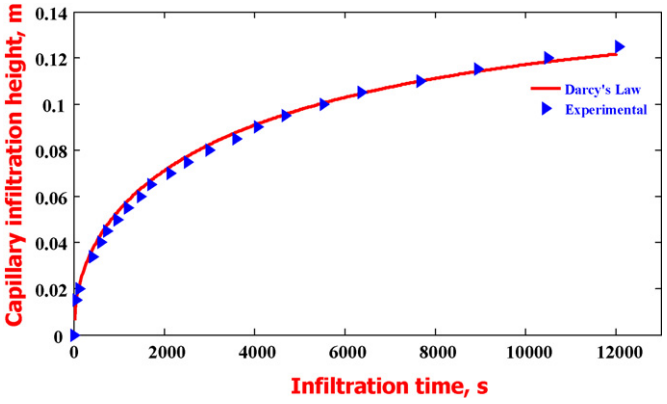

Fig. 11. Comparison of estimated and experimental capillary heights of ethyl alcohol.

Eq. (15) was solved for 'h' as a function of 't'. The estimated and experimental values of infiltration height for all the four solvents have been shown in Figs. 10, 12–14. There is a good agreement.

3.3. Comparison between the two approaches: modified Washburn equation and Darcy's law

From Figs. 10–14, it is inferred that infiltration height estimated by Eqs. (10) and (15) agree very well with the experimental values. Although each equation represents a different physical

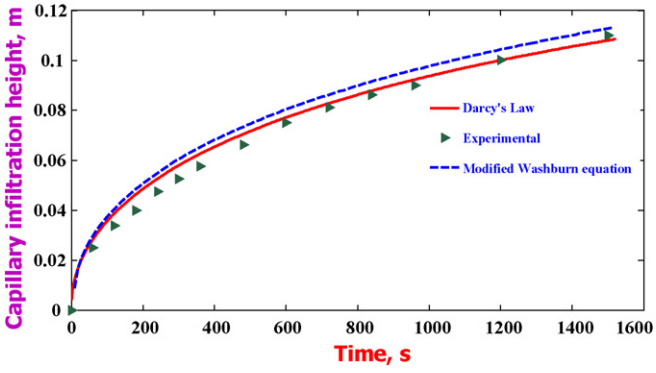

Fig. 12. Comparison of infiltration heights estimated by modified Washburn equation and Darcy's law with experimental values (acetone).

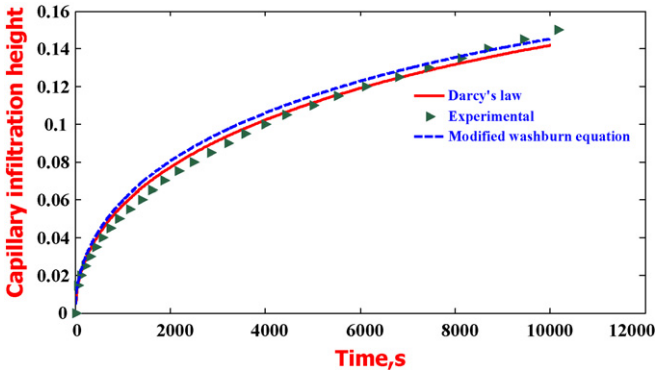

Fig. 13. Comparison of infiltration heights estimated by modified Washburn equation and Darcy's law with experimental values (cyclohexanone).

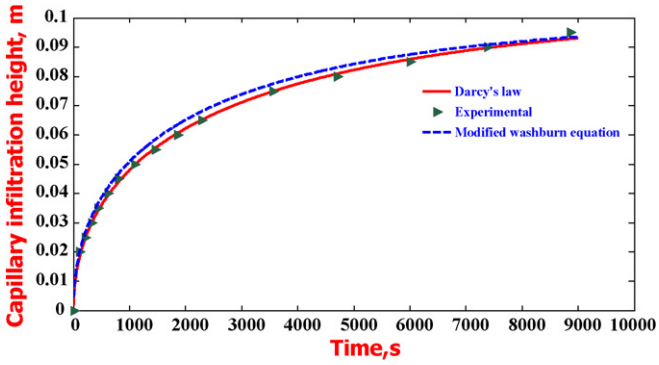

Fig. 14. Comparison of infiltration heights estimated by modified Washburn equation and Darcy's law with experimental values (cyclohexane).

picture, mathematically both are similar: ΔP and κ in Eq. (10) respectively correspond to $(2\sigma\cos\theta)/r_1$ and $r_2^2/8$ in Eq. (15).

4. Concluding remarks

(1) *Porosimetry studies*: There is a wide pore-size distribution in the C–C preforms: 0.007–400 μm. The median pore diameter is 8.6 μm.
(2) *Permeability studies*: The permeability of the C–C preforms was found to be about 2.0×10^{-12} m^2. The solvent infiltration could be correlated by Darcy's law for upward flow using this value of permeability.
(3) *Solvent infiltration studies*:
   (1) The pores in the C–C preforms may be classified as
      (i) Coarse pores existing mainly in the carbon matrix in-between the fabric layers;
      (ii) Fine pores existing mainly in the carbon matrix entrapped in the fabric layers.
   (2) Capillary pressure for solvent infiltration is governed by coarse pores (effective mean radius, $r_1 = 34.2$ μm).
   (3) The rate of infiltration is controlled by all the pores; these may be represented by the median pore size (effective mean radius, $r_2 = 4.3$ μm).
   (4) The kinetics of solvent infiltration can be analyzed by modified Washburn equation based on the above two radii r_1 and r_2.

In the Part B, studies on kinetics of silicon infiltration have been presented.

References

1. Chawla, K. K., *Ceramic Matrix Composites* (*2nd edition*). Kluwer Academic Publishers, 2003, pp. 417–419.
2. Bansal, N. P., *Hand Book of Ceramic Composites*. Kluwer Academic Publishers, 2005, pp. 117–147.
3. Krenkel, W., Carbon-fiber reinforced CMC for high performance structures. *Int. J. Appl. Ceram. Tech.*, 2004, **1**, 188–200.
4. Krenkel, W., In *From Polymer to Ceramics: Low Cost Manufacturing of CMC Materials Fifth International Conference on Frontiers of Polymer and Advanced Materials (ICFPAM)*, 1999.
5. Messner, R. P. and Chiang, Y. M., Liquid-phase reaction-bonding of silicon carbide using alloyed silicon-molybdenum melts. *J. Am. Ceram. Soc.*, 1990, **73**, 1193–1200.
6. Darcy, H. P. G., *Les fontaines publiques de la ville de Dijon, Expositionet application des principles a suivre et des formules a employer dans les questions de distribution d'eau*. Victor Dalmont, Paris, 1856.
7. Einset, E. O., Capillary infiltration rates into porous media with applications to silicomp processing. *J. Am. Ceram. Soc.*, 1996, **79**, 333–338.
8. Sangsuwan, P., Tewari, S. N., Gatica, J. E., Singh, M. and Dickerson, R., Reactive infiltration of silicon melt through microporous amorphous carbon preform. *Metall. Mater. Trans. B*, 1999, **30b**, 933–944.
9. Washburn, E. W., The dynamics of capillary flow. *Phys. Rev.*, 1921, **17**, 273–283.
10. Daniel, B. S. S., Mazumdar, D. and Murthy, V. S. R., Modeling of composite growth in the directed aluminum melt nitridation process. *Metall. Mater. Trans. A*, 1999, **30A**, 2951–2958.
11. Dullien, F. A. L., *Porous Media: Fluid Transport and Pore Structure*. Academic, New York, NY, 1979, p. 119.
12. Trong, D.-V. and Hupka, J., Characterization of porous materials by capillary rise method. *Physicochem. Probl. Min. Process.*, 2005, **39**, 47–65.
13. Suresh and Advani, G., *Process Modeling in Composite Manufacturing*. Marcel Dekker, 2003, pp. 151–161.
14. Abraham, M. and Ruben, D. C., Characterization of porous media by the kinetics of liquid penetration: the vertical capillaries model. *J. Colloid Interface Sci.*, 1997, **189**, 299–304.
15. Perry, Robert H., *Perry's Chemical Engineers' Handbook* (*sixth edition*)., 1984, pp. 3-1–3-291.
16. Asthana, R., An analysis for spreading kinetics of liquid metals on solids. *Metall. Mater. Trans. A*, 1995, **26A**, 1307–1310.
17. Asthana, R., Interface- and diffusion-limited capillary rise of reactive melts with a transient contact angle. *Metall. Mater. Trans. A*, 2002, **33A**, 2119–2128.